The $\pi N \to \pi\pi N$ reaction around the $N^*(1440)$ energy

Hiroyuki Kamano* and Masaki Arima†

Department of Physics, Osaka City University, Osaka 558-8585, Japan

(Received 19 January 2006; published 15 May 2006)

We study the $\pi N \to \pi\pi N$ reaction around the $N^*(1440)$ mass-shell energy. Considering the total cross sections and invariant mass distributions, we discuss the role of $N^*(1440)$ and its decay processes on this reaction. The calculation is performed by extending our previous approach [Phys. Rev. C **69**, 025206 (2004)], in which only the nucleon and $\Delta(1232)$ were considered as intermediate baryon states. The characteristics in the recent data of the $\pi^- p \to \pi^0\pi^0 n$ reaction measured by Crystal Ball Collaboration can be understood as a strong interference between the two decay processes: $N^*(1440) \to \pi\Delta$ and $N^*(1440) \to N(\pi\pi)_{S\,\text{wave}}^{I=0}$. It is also found that the scalar-isoscalar $\pi\pi$ rescattering effect in the $NN^*(\pi\pi)_{S\,\text{wave}}^{I=0}$ vertex, which corresponds to the propagation of σ meson, seems to be necessary for explaining the several observables of the $\pi N \to \pi\pi N$ reaction: the large asymmetric shape in the $\pi^0\pi^0$ invariant mass distributions of the $\pi^- p \to \pi^0\pi^0 n$ reaction and the $\pi^+ p \to \pi^+\pi^+ n$ total cross section.

I. INTRODUCTION

In many pion-induced reactions on the nucleon, the single-pion production reaction $\pi N \to \pi\pi N$ has been studied with a particular interest because of its role as a major inelastic process. The partial-wave analyses of this reaction, together with other reaction channels such as the elastic and $\pi N \to \eta N$ reactions, have revealed various properties of the nonstrange baryon resonances, N^*s and Δs (e.g., see Refs. [1–3]). A number of theoretical investigations have also been performed on the basis of the phenomenological approaches using the effective Lagrangian [4–8] and the chiral perturbation theory [9–12].

In Ref. [13], we have discussed the total cross sections of this reaction up to $T_\pi = 400$ MeV, making use of the chiral reduction formula proposed by Yamagishi and Zahed [14]. We focused on the role of $\Delta(1232)$, i.e., the influence of $\pi\Delta\Delta$ and $\rho N\Delta$ interactions on the reaction processes. Because these interactions are not directly observed through the two-body decay of $\Delta(1232)$ in contrast to the $\pi N\Delta$ interaction, their coupling constants are difficult to determine. We found that the $\pi^\pm p \to \pi^\pm \pi^0 p$ reactions are sensitive to the $\pi\Delta\Delta$ and $\rho N\Delta$ interactions and could be a source of information of their coupling constants.

In addition to being useful for clarifying the properties of $\Delta(1232)$, the $\pi N \to \pi\pi N$ reaction is expected to provide us valuable information about the Roper resonance $N^*(1440)$ and its decay to the $\pi\pi N$ channel. $N^*(1440)$ decays to the $\pi\pi N$ channel via the $N^*(1440) \to \pi\Delta$ and $N^*(1440) \to N(\pi\pi)_{S\,\text{wave}}^{I=0}$ processes, which have the branching ratios of about 25% and 7.5%, respectively [15]. The importance of the latter process has already been pointed out in several studies [4,9].

The importance of $N^*(1440)$ and its subsequent decays has been discussed extensively also in the $pp \to pp\pi^+\pi^-$ and $pn \to d(\pi\pi)^{I=0}$ reactions [16–20]. However, such two-pion decay of $N^*(1440)$ is not easy to study in the elastic $\pi N \to \pi N$ scattering and in the $\gamma N \to \pi\pi N$ reaction because $N^*(1440)$ has small electromagnetic transition rate compared to other relevant resonances such as $\Delta(1232)$ and $N^*(1520)$ [21].

Recently, the $\pi^- p \to \pi^0\pi^0 n$ reaction has been measured up to $p_{\pi^-} = 750$ MeV/c (i.e., $T_\pi \sim 620$ MeV) by Crystal Ball Collaboration (CBC) [22,23]. These high-precision data cover the energy region far from the threshold, in particular around the $N^*(1440)$ mass-shell energy, $T_\pi \sim 480$ MeV. Several new interesting results related to $N^*(1440)$ and its decay processes were reported: (i) The energy dependence of the total cross section shows a shoulderlike shape just below the $N^*(1440)$ energy (see Fig. 14 in Ref. [23], and it should be compared with the $\gamma p \to \pi^0\pi^0 n$ total cross section displayed in the same figure, for which no such shape appears because of the small radiative coupling of $N^*(1440)$). (ii) The $\pi^0 n$ invariant mass distribution shows a peak near the invariant mass equal to the $\Delta(1232)$ energy, which would be produced via the process $N^*(1440) \to \pi\Delta$. (iii) The $\pi^0\pi^0$ invariant mass distributions shows a large asymmetric shape in population of the events, i.e., the peak at large value of $m^2(\pi^0\pi^0)$ is larger than that at small value of $m^2(\pi^0\pi^0)$.

When the total energy increases, the correlation between the outgoing pions will become visible. The scalar-isoscalar correlation of two pions via the $N^*(1440) \to N(\pi\pi)_{S\,\text{wave}}^{I=0}$ decay is particularly interesting, because such correlation may generate the σ meson pole. In view of the sizable contribution of $N^*(1440) \to N(\pi\pi)_{S\,\text{wave}}^{I=0}$, the $\pi N \to \pi\pi N$ reaction is a possible source of information about this controversial scalar meson. It is worth noting that several literatures have suggested that this "σ" degree of freedom is important also in understanding the structure of $N^*(1440)$ [24,25].

In this article, we investigate the $\pi N \to \pi\pi N$ reaction in the energy region up to $T_\pi = 620$ MeV, especially around the

---

*Present address: Department of Physics, Osaka University, Toyonaka, Osaka 560-0043, Japan. Electronic address: kamano@ocunp.hep.osaka-cu.ac.jp

†Electronic address: arima@ocunp.hep.osaka-cu.ac.jp

$N^*(1440)$ mass-shell energy. Through the comparison with the recent CBC data, we particularly discuss the role of $N^*(1440)$ and its decay processes on this reaction. Furthermore, we try to discuss the possibility of extracting the information about the σ meson such as its existence. The calculation is performed by extending and improving the theoretical framework of our previous study [13] in which the contributions of $\Delta(1232)$ have been discussed in detail in the energy region up to $T_\pi = 400$ MeV.

This article is organized as follows. In Sec. II, we give a brief summary of our previous study and explain new ingredients introduced in this work. The numerical results are presented in Sec. III and the contributions of $N^*(1440)$ to the $\pi N \to \pi\pi N$ reaction are discussed. Then our results are compared with the recent CBC data. Summary and conclusions are given in Sec. IV. In the appendices we summarize some details of phenomenological treatment in the calculation.

II. THEORETICAL TREATMENT OF $\pi N \to \pi\pi N$ REACTION

A. Brief summary of our previous study

The starting point of our previous study [13] is the chiral Ward identity satisfied by the invariant amplitude $\mathcal{M}_{\pi\pi N}$. Assigning the four-momentum and isospin indices of the external nucleons and pions as in Fig. 1, we have

$$\mathcal{M}_{\pi\pi N} = (\mathcal{M}_\pi + \mathcal{M}_A + \mathcal{M}_{SA} + \mathcal{M}_{VA}) + (k_1, a \leftrightarrow -k_3, c)$$
$$+ (k_2, b \leftrightarrow k_3, c) + \mathcal{M}_{AAA}, \quad (1)$$

where the symbol ($\leftrightarrow$) represents a permutation of the momentum and isospin indices of the pion in the first four terms, and

$$\mathcal{M}_\pi = \frac{1}{f_\pi^2}\big[(k_1 - k_2)^2 - m_\pi^2\big]\delta^{ab}\langle N(p_2)|\hat{\pi}^c(0)|N(p_1)\rangle, \quad (2)$$

$$\mathcal{M}_A = -\frac{i}{2f_\pi^3}(k_2 - k_1)^\mu \delta^{ab}\langle N(p_2)|j_{A\mu}^c(0)|N(p_1)\rangle, \quad (3)$$

$$\mathcal{M}_{SA} = -\frac{m_\pi^2}{f_\pi^2}k_3^\mu \delta^{ab}\int d^4x\, e^{-i(k_1-k_2)x}$$
$$\times \langle N(p_2)|T^*\big[\hat{\sigma}(x)j_{A\mu}^c(0)\big]|N(p_1)\rangle, \quad (4)$$

$$\mathcal{M}_{VA} = -\frac{i}{2f_\pi^3}(k_1 + k_2)^\mu k_3^\nu \varepsilon^{abe}\int d^4x\, e^{-i(k_1-k_2)x}$$
$$\times \langle N(p_2)|T^*\big[j_{V\mu}^e(x)j_{A\nu}^c(0)\big]|N(p_1)\rangle, \quad (5)$$

$$\mathcal{M}_{AAA} = \frac{i}{f_\pi^3}k_1^\mu k_2^\nu k_3^\lambda \int d^4x_1 d^4x_2\, e^{-ik_1x_1 + ik_2x_2}$$
$$\times \langle N(p_2)|T^*\big[j_{A\mu}^a(x_1)j_{A\nu}^b(x_2)j_{A\lambda}^c(0)\big]|N(p_1)\rangle. \quad (6)$$

The pseudoscalar density $\hat{\pi}^a(x)$ is the interpolating pion field with the asymptotic form $\hat{\pi}^a(x) \to \pi_{\text{in,out}}(x) + \cdots$ ($x_0 \to \mp\infty$). The one-pion reduced axial current $j_{A\mu}^a(x)$ is defined by $j_{A\mu}^a(x) = A_\mu^a(x) + f_\pi \partial_\mu \hat{\pi}^a(x)$, where $A_\mu^a(x)$ is the ordinary axial current with the asymptotic form $A_\mu^a(x) \to -f_\pi \partial_\mu \pi_{\text{in,out}}(x) + \cdots (x_0 \to \mp\infty)$. The vector current and the scalar density are represented by $j_{V\mu}^a(x)$ and $\hat{\sigma}(x)$, respectively.
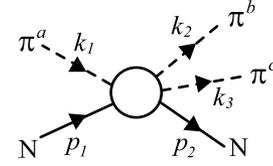
FIG. 1. The $\pi N \to \pi\pi N$ reaction. Pions have the isospin index (a, b, c) and the four-momentum k_i ($i = 1, 2, 3$), and nucleons have the four-momentum p_j ($j = 1, 2$).

The Ward identity [Eqs. (1)–(6)] was first derived by Yamagishi and Zahed making use of the chiral reduction formula [14,26]. Owing to this formula the invariant amplitude is expressed in terms of Green's functions of well-defined current and density operators. Then the consequences of broken chiral symmetry subject to the asymptotic condition $\partial^\mu A_\mu^a(x) \to f_\pi m_\pi^2 \pi_{\text{in,out}}(x) + \cdots (x_0 \to \mp\infty)$ are exactly embodied on the amplitude without relying on any specific model or expansion scheme. Thus, by using the chiral reduction formula at the beginning of the discussion, we can consider the detail of each reaction mechanism separately from the general framework required by broken chiral symmetry. This nature of the chiral reduction formula has a great advantage in tackling on the hadronic processes in the resonance region in which the systematic chiral expansion scheme becomes difficult to be implemented.

Green's functions (i.e., the matrix elements of current and density operators) appearing in Eqs. (2)–(6) are not uniquely determined by broken chiral symmetry. Therefore we need to employ a model to evaluate Green's functions. In Ref. [13] they were calculated by taking a phenomenological approach based on the relativistic tree-level diagrams as shown in Fig. 2. We considered only the nucleon and $\Delta(1232)$ as the intermediate
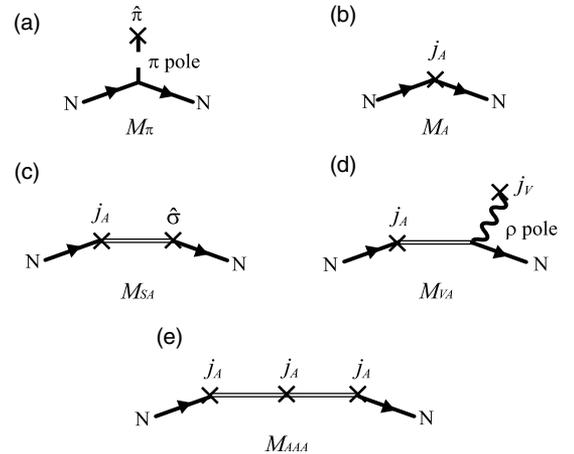
FIG. 2. The diagrams considered in our previous study [13] to evaluate Green's functions in Eqs. (2)–(6). Crossed versions are also considered for all of these diagrams. The double line represents the propagation of the nucleon or $\Delta(1232)$. Note that $\Delta(1232)$ does not propagate in $\mathcal{M}_{SA}$ because the N-Δ transition is not brought about by the scalar-density operator $\hat{\sigma}$. The pseudoscalar density $\hat{\pi}$ and the vector current j_V are dominated by the pion and ρ meson pole, respectively.

baryons, and π and ρ as the intermediate mesons. Details of our model [13] are summarized in Appendix A.

B. Contribution of $N^*(1440)$

Now we extend our previous approach by including $N^*(1440)$. As for the contributions of $N^*(1440)$ on the reaction, we consider the $\pi N N^*$, $N N^*(\pi\pi)_{S\,\text{wave}}^{I=0}$, and $\pi \Delta N^*$ interactions. The first two interactions have already been considered in many theoretical investigations of the $\pi N \to \pi\pi N$ reaction near threshold. Although the $\pi \Delta N^*$ interaction has often been neglected, this interaction will become important in the energy region considered in this article: Indeed, the importance of $N^* \to \Delta\pi$ decay is suggested experimentally [22,23].

1. $\pi N N^*$ and $\pi \Delta N^*$ interactions

The $\pi N N^*$ and $\pi \Delta N^*$ vertices with the one-pion leg are generally related to the matrix elements of axial current $j_{A\mu}^a$ for the N-N^* transition as

$$\langle N(p')|j_{A\mu}^a(0)|N^*(p)\rangle$$
$$= \bar{u}_N(p')\left[F_{A,1}^{NN^*}(t)\gamma_\mu + F_{A,2}^{NN^*}(t)q_\mu\right]\gamma_5 \frac{\tau^a}{2} u_{N^*}(p) \quad (7)$$

and for the Δ-N^* transition as

$$\langle \Delta(p')|j_{A\mu}^a(0)|N^*(p)\rangle$$
$$= \bar{U}^\nu(p')\left[F_{A,1}^{\Delta N^*}(t)g_{\nu\mu} + F_{A,2}^{\Delta N^*}(t)Q_\nu\gamma_\mu + F_{A,3}^{\Delta N^*}(t)Q_\nu Q_\mu \right.$$
$$\left. + F_{A,4}^{\Delta N^*}(t)Q_\nu i\sigma_{\mu\lambda}Q^\lambda\right]I^a\left(\tfrac{3}{2},\tfrac{1}{2}\right)u_{N^*}(p), \quad (8)$$

respectively, where $q^\mu = (p'-p)^\mu$, $Q^\mu = -q^\mu$, and $t = (p'-p)^2$; τ^a is the isospin Pauli matrix; and $I^a(i,j)$ is the $j \to i$ isospin transition $(2i+1)\times(2j+1)$ matrix. The isoquadruplet Rarita-Schwinger vector-spinor and the isodoublet Dirac spinor are denoted as $U^\mu(p)$ and $u_i(p)$ $(i = N, N^*)$, respectively. By employing Eqs. (B5) and (B6) as the effective $\pi N N^*$ and $\pi \Delta N^*$ interactions, some of the form factors in Eqs. (7) and (8) can be exactly related to the renormalized coupling constants

$$f_{\pi N N^*}(t) = \frac{m_\pi}{f_\pi}\left[\frac{1}{2}F_{A,1}^{NN^*}(t) + \frac{t}{4m_{N^*}}F_{A,2}^{NN^*}(t)\right], \quad (9)$$

$$f_{\pi \Delta N^*}(t) = \frac{m_\pi}{f_\pi}\left[F_{A,1}^{\Delta N^*}(t) + (m_{N^*}-m_\Delta)\right.$$
$$\left. \times F_{A,2}^{\Delta N^*}(t) + tF_{A,3}^{\Delta N^*}(t)\right]. \quad (10)$$

At tree level, all the form factors are reduced to constants. Because it is difficult to fix all of their value in the present status of experimental data, we eliminate $F_{A,2}^{NN^*}$ and $F_{A,3}^{\Delta N^*}$ by using the PCAC hypothesis $f_{\pi NN^*,\pi\Delta N^*}(m_\pi^2) \simeq f_{\pi NN^*,\pi\Delta N^*}(0)$. Then, at tree level, we obtain the analogs of Goldberger-Treiman relation for the $\pi N N$ interaction,

$$f_{\pi N N^*}(m_\pi^2) = \frac{m_\pi}{2f_\pi}F_{A,1}^{NN^*} \quad (11)$$

and

$$f_{\pi \Delta N^*}(m_\pi^2) = \frac{m_\pi}{f_\pi}\left[F_{A,1}^{\Delta N^*} + (m_{N^*}-m_\Delta)F_{A,2}^{\Delta N^*}\right], \quad (12)$$

respectively.

Furthermore, in this article we neglect $F_{A,2}^{\Delta N^*}$ for simplicity. This would be partly justified by the fact that, in the case of $\pi N \Delta$ interaction, the contribution of the $F_{A,2}$ term is considerably small compared to the $F_{A,1}$ term [13]. The form factor $F_{A,4}^{\Delta N^*}(t)$ does not appear in our calculation as long as we consider the Lagrangian (B6) for the $\pi \Delta N^*$ interaction.

Using the central values of the $N^*(1440) \to \pi N$ and $N^*(1440) \to \pi \Delta$ decay widths listed in the particle data table of Ref. [15], we obtain $f_{\pi NN^*}(m_\pi^2) = 0.465$ and $f_{\pi \Delta N^*}(m_\pi^2) = 1.71$. As for $f_{\pi \Delta N^*}(m_\pi^2)$, we take account of the finite width of $\Delta(1232)$ in the same manner as in Ref. [21]. Those values lead to $F_{A,1}^{NN^*} = 0.63$ and $F_{A,1}^{\Delta N^*} = 1.15$, respectively.

2. $NN^*(\pi\pi)_{S\,wave}^{I=0}$ interaction

We next consider the $NN^*(\pi\pi)_{S\,\text{wave}}^{I=0}$ interaction with the two-pion leg. Recently, we have discussed in detail its general and phenomenological aspects on the basis of chiral reduction formula [27]. We make use of our results also in the present work.

Using the chiral reduction formula, we find that the $NN^*(\pi\pi)_{S\,\text{wave}}^{I=0}$ vertex is generally described by the following matrix elements of currents and density operators (see Fig. 3). One is the scalar matrix element of the N-N^* transition [Fig. 3(a)], which is factorized as

$$\langle N(p')|\hat{\sigma}(0)|N^*(p)\rangle = -\frac{\sigma_{\text{RN}}(t)}{f_\pi m_\pi^2}\bar{u}_N(p')u_{N^*}(p). \quad (13)$$

Another is the matrix element of the N-N^* transition caused by the contact, scalar-isoscalar combination of two axial currents [Fig. 3(b)], which is expressed as

$$\int d^4x e^{ikx}\langle N(p')|T^*\left(j_{A\mu}^a(x)j_{A\nu}^b(0)\right)|N^*(p)\rangle\Big|_{\text{scalar-contact}}$$
$$= -i\delta^{ab}g_{\mu\nu}F_{\text{AA}}(t)\bar{u}_N(p')u_{N^*}(p), \quad (14)$$

where k represents the four-momentum of external pion with the isospin index a. Note that $F_{\text{AA}}(t)$ does not contain
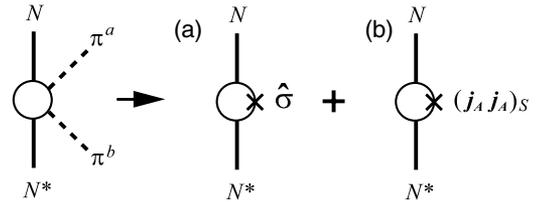
FIG. 3. The diagrammatical interpretation for the chiral reduction of the $NN^*(\pi\pi)_{S\,\text{wave}}^{I=0}$ vertex. The decay amplitude is decomposed into two contributions arising from the different origin in the chiral structure: one includes (a) the scalar N^*-N transition matrix element and another includes (b) the N^*-N transition matrix element of the contact, scalar-isoscalar combination of two axial currents. The former is because of the explicit breaking of chiral symmetry and thus vanishes in the chiral limit, whereas the latter does not.
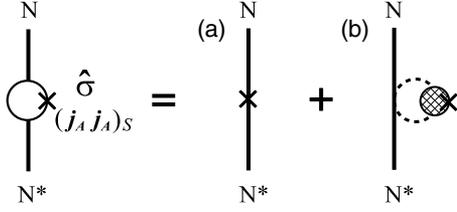
FIG. 4. The "minimal model" for the $NN^*(\pi\pi)^{I=0}_{S\,\mathrm{wave}}$ vertex. The form factors $\sigma_{\mathrm{RN}}(t)$ and $F_{\mathrm{AA}}(t)$ are dominated by the processes: (a) the contact term and (b) the $\pi\pi$ rescattering together with the contact scalar-isoscalar baryon-pion interaction (the meshed blob represents $\pi\pi$ rescattering in the $I = J = 0$ channel).

any single baryon poles owing to the definition for the $N^*(1440) \rightarrow N(\pi\pi)^{I=0}_{S\,\mathrm{wave}}$ decay given in Ref. [15]. We then obtain the general expression for the $NN^*(\pi\pi)^{I=0}_{S\,\mathrm{wave}}$ vertex as

$$\mathcal{M}_{NN^*(\pi\pi)_S} = \frac{\delta^{ab}}{f_\pi^2} \left[\sigma_{\mathrm{RN}}(t) - \frac{t - 2m_\pi^2}{2} F_{\mathrm{AA}}(t) \right]$$
$$\times \bar{u}_N(p') u_{N^*}(p). \quad (15)$$

When $\sigma_{\mathrm{RN}}(t)$ and $F_{\mathrm{AA}}(t)$ are constants, this expression reduces to the result obtained from the effective chiral Lagrangian to order q^2 [9].

Instead of taking $\sigma_{\mathrm{RN}}(t)$ and $F_{\mathrm{AA}}(t)$ as constants, we proposed in Ref. [27] the "minimal model," which explicitly includes the scalar-isoscalar correlation of two-pions by considering the $\pi\pi$ rescattering mechanism in $I = J = 0$ channel (Fig. 4). This model gives the following parametrizations of $\sigma_{\mathrm{RN}}(t)$ and $F_{\mathrm{AA}}(t)$,

$$\sigma_{\mathrm{RN}}(t) \rightarrow \sigma_{\mathrm{RN}} \times \left[1 + \tfrac{1}{6} G(t) t^{I=0}_{\pi\pi}(t) \right], \quad (16)$$

$$F_{\mathrm{AA}}(t) \rightarrow F_{\mathrm{AA}} \times \left[1 + \tfrac{1}{6} G(t) t^{I=0}_{\pi\pi}(t) \right], \quad (17)$$

where $G(t)$ and $t^{I=0}_{\pi\pi}(t)$ are the pion loop integral and $I = 0$ $\pi\pi$ rescattering amplitude,

$$G(t) = i \int \frac{d^4 l}{(2\pi)^4} \frac{1}{l^2 - m_\pi^2 + i\varepsilon} \frac{1}{(l - P)^2 - m_\pi^2 + i\varepsilon} \quad (18)$$

with $P^2 = t$, and

$$t^{I=0}_{\pi\pi}(t) = -\frac{6}{f_\pi^2} \frac{t - m_\pi^2/2}{1 + (1/f_\pi^2)(t - m_\pi^2/2) G(t)}, \quad (19)$$

respectively [27]. Based on the dimensional regularization scheme with a renormalization scale $\mu = 1.2$ GeV, the loop integral $G(t)$ can be expressed as

$$G(t) = \frac{1}{(4\pi)^2} \left(-1 + \ln \frac{m_\pi^2}{\mu^2} + \sigma \ln \frac{1 + \sigma}{1 - \sigma} - i\pi\sigma \right) \quad (20)$$

for $t > 4m_\pi^2$,

$$G(t) = \frac{1}{(4\pi)^2} \left(-1 + \ln \frac{m_\pi^2}{\mu^2} + \sigma \ln \frac{\sigma + 1}{\sigma - 1} \right) \quad (21)$$

for $t < 0$, and

$$G(t) = \frac{1}{(4\pi)^2} \left[-1 + \ln \frac{m_\pi^2}{\mu^2} + \sigma(\pi - 2\arctan\sigma) \right] \quad (22)$$

for $0 < t < 4m_\pi^2$, where $\sigma = \sqrt{|1 - (4m_\pi^2/t)|}$.

Using Eqs. (15)–(17) and performing the phase-space integral, we obtain the following expression for the $N^*(1440) \rightarrow N(\pi\pi)^{I=0}_{S\,\mathrm{wave}}$ decay width

$$\Gamma_{NN^*(\pi\pi)_S} = \alpha(c_1^*)^2 + \beta(c_2^*)^2 + \gamma c_1^* c_2^*, \quad (23)$$

where $c_1^* = -\sigma_{\mathrm{RN}}/(2m_\pi^2)$ and $c_2^* = F_{\mathrm{AA}}/2$. The numerical value of the coefficients α, β, and γ is $\alpha = 1.199 \times 10^{-3}$ GeV^3, $\beta = 14.06 \times 10^{-3}$ GeV^3, and $\gamma = 7.754 \times 10^{-3}$ GeV^3, respectively. We note that these values are different from those of Refs. [9,16]. This difference arises from the $\pi\pi$ rescattering and the relativistic effects. Both c_1^* and c_2^* are not fixed by the $N^*(1440) \rightarrow N(\pi\pi)^{I=0}_{S\,\mathrm{wave}}$ decay width, and we can take any value on the ellipse (23) on the c_1^*-c_2^* plane.

C. Cutoff factor

We shall introduce the cutoff factors, which stem from the finite size of hadrons, for each vertex in a phenomenological manner. In Ref. [13] we treated all hadrons as the pointlike particles. They are, however, the bound states of quarks and gluons and thus have the finite size. Although in principle those effects should be directly derived from QCD, it is very difficult and still an open question which deserves the theoretical challenges. Instead, we consider those effects phenomenologically according to the discussions of Ref. [28]. We attach the four-dimensional cutoff factors,

$$f_\alpha(p_\alpha^2) = \frac{\Lambda_\alpha^4}{\Lambda_\alpha^4 + (p_\alpha^2 - m_\alpha^2)^2}, \quad (24)$$

to each leg α of the vertex (where we assume $n_\alpha = 1$ [28]). Here p_α and m_α are the four-momentum and mass of the particle corresponding to the leg α, respectively. The cutoff factor f_α is normalized to one on the mass-shell, and thus exhibits its effect only for the internal lines. There are five cutoff parameters: Λ_N, Λ_Δ, and Λ_{N^*} for the intermediate baryons, and Λ_π and Λ_ρ for the pion and ρ meson poles appearing in Figs. 2(a) and 2(d). In this article we assume $\Lambda_N = \Lambda_\Delta = \Lambda_{N^*} \equiv \Lambda_B$ and $\Lambda_\pi = \Lambda_\rho \equiv \Lambda_M$.

III. RESULTS AND DISCUSSIONS

Putting together all diagrams introduced in our previous study (Fig. 2) and this work (Fig. 5), we calculate the $\pi N \rightarrow \pi\pi N$ total cross sections up to $T_\pi = 620$ MeV. We also calculate the $\pi^0\pi^0$ and $\pi^0 n$ invariant mass distributions for the $\pi^- p \rightarrow \pi^0\pi^0 n$ reactions whose experimental data were reported by CBC [23]. We especially try to discuss the contributions of $N^*(1440)$ around its mass-shell energy.

(a)

(b)

(c)
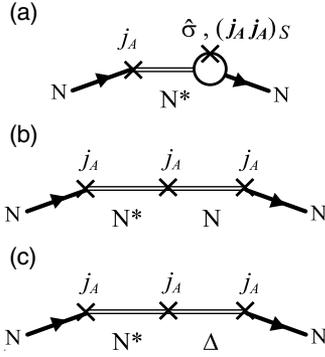
FIG. 5. The diagrams including $N^*(1440)$ taken into account in the present article. All crossed versions of these diagrams are also considered.

A. Fixing parameters

Before showing our results, we mention how to fix the parameters: the cutoff parameters Λ_B and Λ_M, and the coupling constants of the $\pi\Delta\Delta$ and $\rho N\Delta$ interactions (denoted as $f_{\pi\Delta\Delta}$ and $f_{\rho N\Delta}$, respectively), and the parameters c_1^* and c_2^* that characterize $NN^*(\pi\pi)_{S\,\text{wave}}^{I=0}$ interaction.

Because the value of $f_{\pi\Delta\Delta}$ and $f_{\rho N\Delta}$ cannot be directly determined by the two-body decay width, they are usually extracted from the data using the meson exchange model or estimated by using theoretical approach such as the quark model and QCD sum rule. Many reports on their value fall into the ranges of $0.4 \lesssim f_{\pi\Delta\Delta} \lesssim 0.8$ and $3.5 \lesssim f_{\rho N\Delta} \lesssim 7.8$ (see [13] and references therein). For instance, the quark model relations lead to $f_{\pi\Delta\Delta} = 0.8$ and $f_{\rho N\Delta} = 5.5$ [29,30].

In Ref. [13], it is found that, at least in the low-energy region up to $T_\pi = 400$ MeV, the influences of the $\pi\Delta\Delta$ and $\rho N\Delta$ interactions are negligible for the $\pi^- p \to \pi^+\pi^- n$ and $\pi^- p \to \pi^0\pi^0 n$ channels. However, the $NN^*(\pi\pi)_{S\,\text{wave}}^{I=0}$ interaction (i.e., c_1^* and c_2^*) gives a negligible contribution to other three channels, i.e., $\pi^\pm p \to \pi^\pm\pi^0 p$ and $\pi^+ p \to \pi^+\pi^+ n$ [4]. This fact allows us to consider $(f_{\rho N\Delta}, f_{\pi\Delta\Delta})$ and (c_1^*, c_2^*) separately in the parameter fixing. Thus we first try to investigate the influences of Λ_B, Λ_M, $f_{\pi\Delta\Delta}$, and $f_{\rho N\Delta}$ on the

total cross sections of $\pi^\pm p \to \pi^\pm\pi^0 p$ and $\pi^+ p \to \pi^+\pi^+ n$ channels and to estimate the value of these parameters.

1. Cutoff dependence

In Fig. 6 we show the cutoff dependence of the total cross sections. In this calculation, we include all diagrams but Fig. 5(a), which includes the $NN^*(\pi\pi)_{S\,\text{wave}}^{I=0}$ vertex, and take $f_{\pi\Delta\Delta} = 0.4$ and $f_{\rho N\Delta} = 7.8$, which are in the range explained above.[1]

First, if we do not take account of the cutoff factor (24) for each leg of the vertices, i.e., if we treat the hadrons as pointlike particle, the resulting total cross sections obviously overshoot the experimental data above $T_\pi \sim 300$ MeV.

We choose three typical values $\Lambda_B = \Lambda_M = 750$, 850, and 950 MeV and calculate the cross sections for each value. As shown in Fig. 6, we can see clear difference among these results above $T_\pi \sim 300$ MeV. For the $\pi^+ p \to \pi^+\pi^+ n$ channel, the case of $\Lambda_B = \Lambda_M = 850$ MeV seems most appropriate. The difference is obviously seen in the results for the $\pi^+ p \to \pi^+\pi^0 p$ channel. The case of $\Lambda_B = \Lambda_M = 950$ MeV is quite different from the data compared to the other two cases. For the $\pi^- p \to \pi^-\pi^0 p$ channel, all results somewhat underestimate the data.

Next we consider several cases of $\Lambda_B \neq \Lambda_M$: $\Lambda_M = 0.5\Lambda_B$, $1.5\Lambda_B$, and $2\Lambda_B$ for each value of Λ_B. As for the $\pi^+ p \to \pi^+\pi^+ n$ and $\pi^+ p \to \pi^+\pi^0 p$ channels the results change only within 10% when we vary the value of Λ_M, whereas the $\pi^- p \to \pi^-\pi^0 p$ channel is sensitive to the variation of Λ_M. We find that the larger value of Λ_M for each Λ_B seems appropriate: the thick solid line in Fig. 6(c) for $\Lambda_B = 850$ MeV and $\Lambda_M = 2\Lambda_B = 1700$ MeV (this line should be compared to the thin solid line with $\Lambda_B = \Lambda_M = 850$ MeV).

In the following discussions, we take $\Lambda_B = 850$ MeV and $\Lambda_M = 1700$ MeV.

---

[1]The reason for taking these values is discussed later.
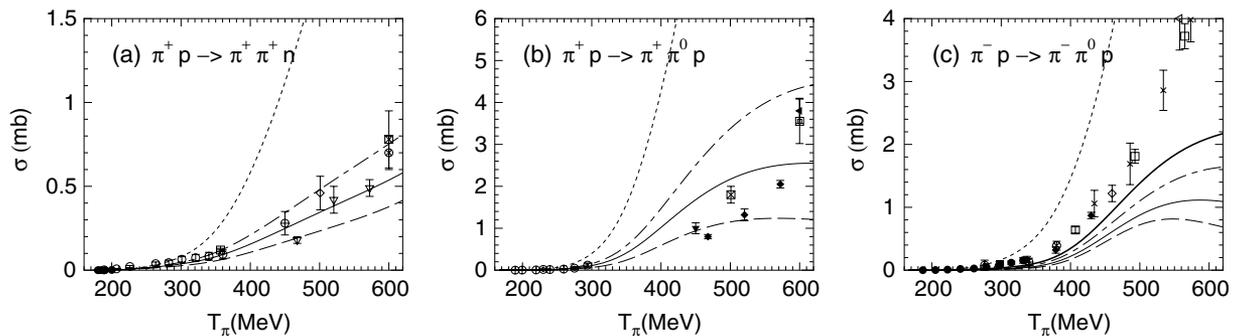
FIG. 6. The cutoff dependence of the total cross sections. The results are shown for the cases of $\Lambda_B = \Lambda_M = 750$ MeV (dashed line), $\Lambda_B = \Lambda_M = 850$ MeV (solid line), and $\Lambda_B = \Lambda_M = 950$ MeV (dashed-dotted line). The results without considering the cutoff factors are shown by the dotted line. The thick solid line in (c) corresponds to the case of $\Lambda_B = 850$ MeV and $\Lambda_M = 2\Lambda_B = 1700$ MeV. The data are from Refs. [31–52].

FIG. 7. The dependence of numerical results on $f_{\pi\Delta\Delta}$ and $f_{\rho N\Delta}$: (a) the $\pi^+ p \to \pi^+ \pi^0 p$ channel with $(f_{\pi\Delta\Delta}, f_{\rho N\Delta}) = (0.4, 7.8)$ (solid line), $(f_{\pi\Delta\Delta}, f_{\rho N\Delta}) = (0.6, 7.8)$ (dashed line), and $(f_{\pi\Delta\Delta}, f_{\rho N\Delta}) = (0.8, 7.8)$ (dotted line) and (b) the $\pi^- p \to \pi^- \pi^0 p$ channel with $(f_{\pi\Delta\Delta}, f_{\rho N\Delta}) = (0.4, 7.8)$ (solid line), $(f_{\pi\Delta\Delta}, f_{\rho N\Delta}) = (0.4, 5.7)$ (dashed line), and $(f_{\pi\Delta\Delta}, f_{\rho N\Delta}) = (0.4, 3.5)$ (dotted line). The contribution of Fig. 5(a) is not taken into account. We use $\Lambda_B = 850$ MeV and $\Lambda_M = 1700$ MeV. The data are the same as in Fig. 6.
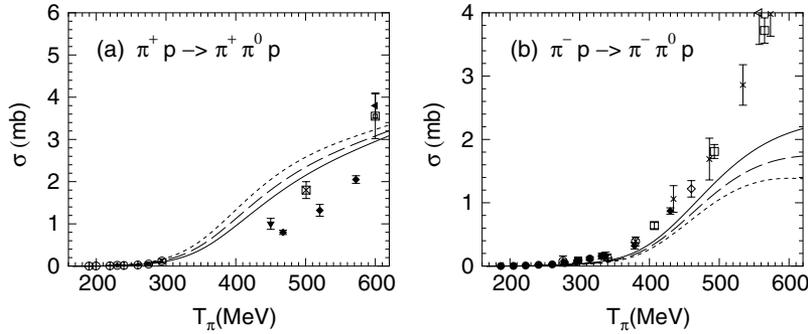
2. The $\pi\Delta\Delta$ and $\rho N\Delta$ interactions

Here we try to examine how the total cross section changes according to the variation of $f_{\pi\Delta\Delta}$ and $f_{\rho N\Delta}$ in their allowed range. For the $\pi^+ p \to \pi^+ \pi^+ n$ channel, the change is small and the results are still compatible with the data. For the $\pi^+ p \to \pi^+ \pi^0 p$ channel, the influence of the $\rho N\Delta$ interaction can be hardly seen for $3.5 \lesssim f_{\rho N\Delta} \lesssim 7.8$, whereas the $\pi\Delta\Delta$ interaction generates visible change on this channel [Fig. 7(a)]. The lower value of $f_{\pi\Delta\Delta}$ seems appropriate to the data. In contrast, for the variation of $f_{\rho N\Delta}$ the change of the $\pi^- p \to \pi^- \pi^0 p$ channel is clearly seen [Fig. 7(b)] but is negligible for that of $f_{\pi\Delta\Delta}$. The higher value of $f_{\rho N\Delta}$ seems appropriate to the data.

This is why we used $f_{\pi\Delta\Delta} = 0.4$ and $f_{\rho N\Delta} = 7.8$ in the discussions of cutoff dependence of the total cross sections. Also in the following we continue to use these values for $f_{\pi\Delta\Delta}$ and $f_{\rho N\Delta}$.

3. The dependence on c_1^* and c_2^*

As mentioned in Sec. II B, the values of c_1^* and c_2^* cannot be fixed by the relation (23) with the decay width of $N^*(1440) \to N(\pi\pi)_{S\,\text{wave}}^{I=0}$, which just represents the ellipse on the c_1^*-c_2^* plane as shown in Fig. 8. Although the case of $c_2^* = 0$ and $c_1^* < 0$ (point A in Fig. 8) is conventionally used in the phenomenological models of hadron reactions (e.g., see Refs. [5,21]), it was first pointed out in Ref. [9] that the c_2^* contribution should be also considered in view of the general chiral effective Lagrangian. Several attempts have been recently performed to determine the values of c_1^* and c_2^* [16,53].

Calculating the total cross sections for all five channels up to $T_\pi = 620$ MeV with allowed values of c_1^* and c_2^*, we find that the appropriate values would be on the solid curve in Fig. 8. The values on the dotted-curve generate obvious disagreement in the total cross section, which is consistent with other studies of the $\pi N \to \pi\pi N$ reaction [4].

In Fig. 9, we show the total cross sections calculated with several values of c_1^* and c_2^* on the solid curve in Fig. 8. The recent CBC data for the $\pi^- p \to \pi^0 \pi^0 n$ channel are plotted as the filled square in Fig. 9(e). We notice the CBC data exhibit a bump below the $N^*(1440)$ energy, i.e., $350 \lesssim T_\pi \lesssim 500$ MeV, and this bump is called the "shoulder" in Ref. [23].

For the $\pi^\pm p \to \pi^\pm \pi^0 p$ channels, the results show only a small increase in the total cross section above $T_\pi = 500$ MeV except for c_1^* and c_2^* around point C [see Figs. 9(b) and 9(c)].

Below $T_\pi = 500$ MeV, however, the $NN^*(\pi\pi)_{S\,\text{wave}}^{I=0}$ interaction has no influence on the total cross section. This result is consistent with other studies [4,13].

However, the $\pi^- p \to \pi^+ \pi^- n$ and $\pi^- p \to \pi^0 \pi^0 n$ channels are sensitive to the variation of c_1^* and c_2^* [Figs. 9(d) and 9(e)]. This fact is expected from other studies at low energy [4,9]. The results with c_1^* and c_2^* near points B and C are obviously incompatible with the experimental data. The preferable value of c_1^* seems to be found between points A and C in view of the data.

The $\pi^+ p \to \pi^+ \pi^+ n$ channel is also sensitive to the variation of c_1^* and c_2^* [see Fig. 9(a)]. The total cross section above $T_\pi = 400$ MeV is increased by the contribution of the process Fig. 5(a): the lower the value of c_1^* becomes, the larger its increase is. Because this channel is, however, already reproduced well without $N^*(1440)$, accurate data of the $\pi^+ p \to \pi^+ \pi^+ n$ reaction above $T_\pi = 400$ MeV will strongly constrain the value of c_1^* and c_2^*. From the current $\pi^+ p \to \pi^+ \pi^+ n$ data, we find that $c_1^* \geqslant -8.0$ GeV^{-1} is preferable in our model.
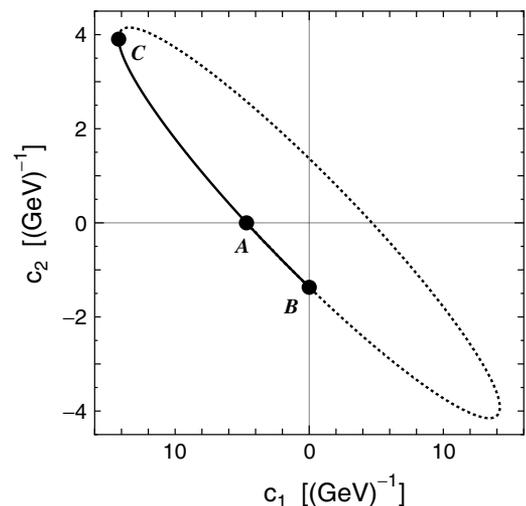
FIG. 8. The ellipse (23) representing the allowed values of c_1^* and c_2^*. Here $\Gamma_{NN^*(\pi\pi)_S} = 26.25$ MeV is used, which is the central value listed in the particle data table [15]. Point A, which is $(c_1^*, c_2^*) = (-4.68, 0)$ GeV^{-1} in our case, corresponds to the point often used in the study of hadron reactions. The points B and C correspond to $(c_1^*, c_2^*) = (0, -1.37)$ GeV^{-1} and $(c_1^*, c_2^*) = (-14.2, 3.92)$ GeV^{-1}, respectively. See the text for the meanings of the solid and dotted parts of this ellipse.
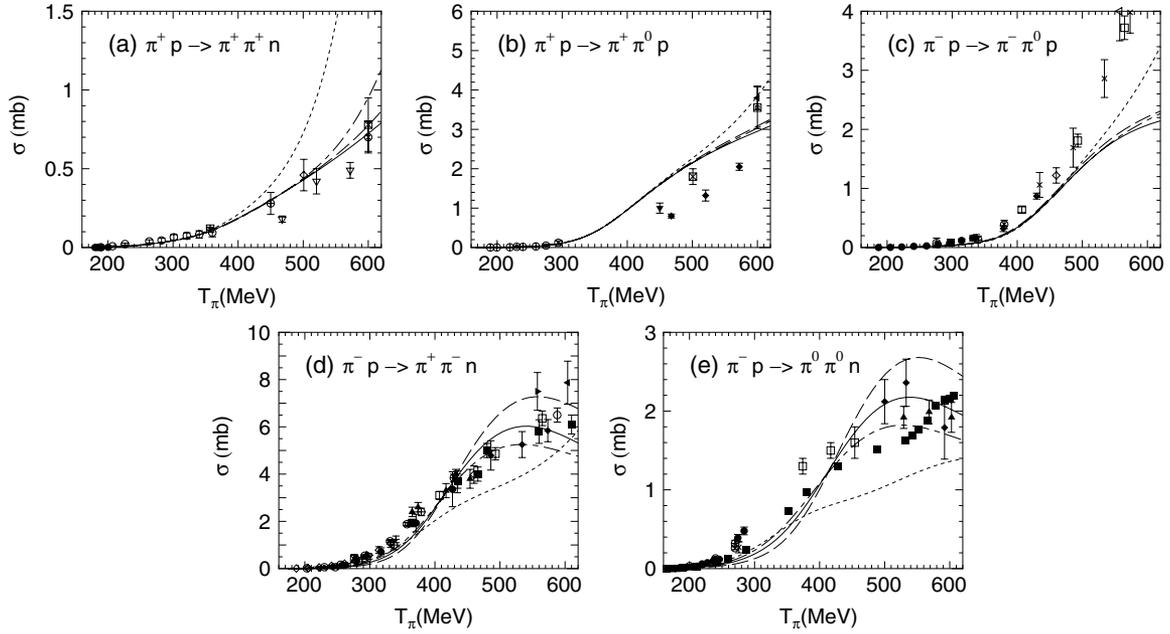
FIG. 9. The c_1^* and c_2^* dependence of the total cross sections. The solid line is the result with (c_1^*, c_2^*) at point A on the ellipse, whereas the dashed and dotted lines are at points B and C, respectively. The dotted-dashed line is for $(c_1^*, c_2^*) = (-8.0, 1.08)$ GeV^{-1}. The data are the same as in Fig. 8 for (a)–(c), whereas for (d) and (e) the data are taken from Refs. [42–49,52,54–69]. The CBC data are plotted as the filled square in (e).

It is worth noting that, in contrast to other three channels, our results for the $\pi^- p \to \pi^+ \pi^- n$ and $\pi^- p \to \pi^0 \pi^0 n$ channels show peak structure around the $N^*(1440)$ energy corresponding to $T_\pi \sim 480$ MeV, except for those with extremely low values of c_1^* near the point C. This feature should be compared with the CBC data for the $\pi^- p \to \pi^0 \pi^0 n$ total cross section, which shows the shoulder at the $N^*(1440)$ energy.
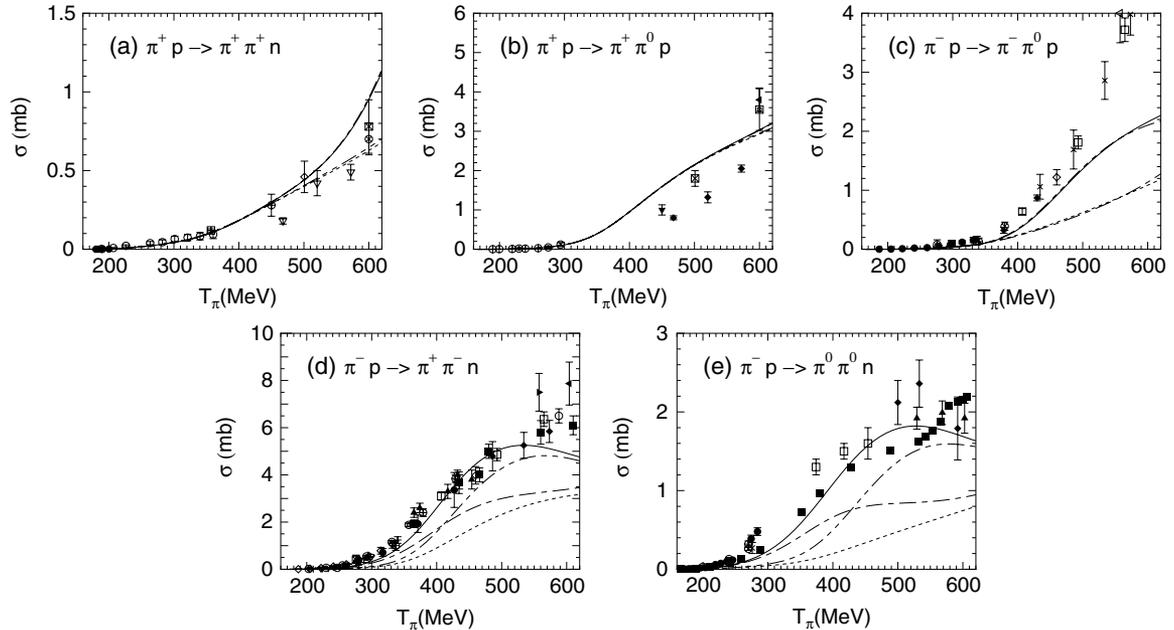
FIG. 10. The contribution of each diagram including $N^*(1440)$ to the total cross sections. The value of (c_1^*, c_2^*) is taken as $(-8.0, 1.08)$ GeV^{-1}. Each line expresses the result, including (i) all diagrams (solid line), (ii) no $\pi \Delta N^*$ vertex (dotted-dashed line), (iii) no $NN^*(\pi\pi)_{S\,\text{wave}}^{I=0}$ vertex (two-dotted-dashed line), and (iv) neither contribution (dotted line). The data are the same as in Fig. 9.
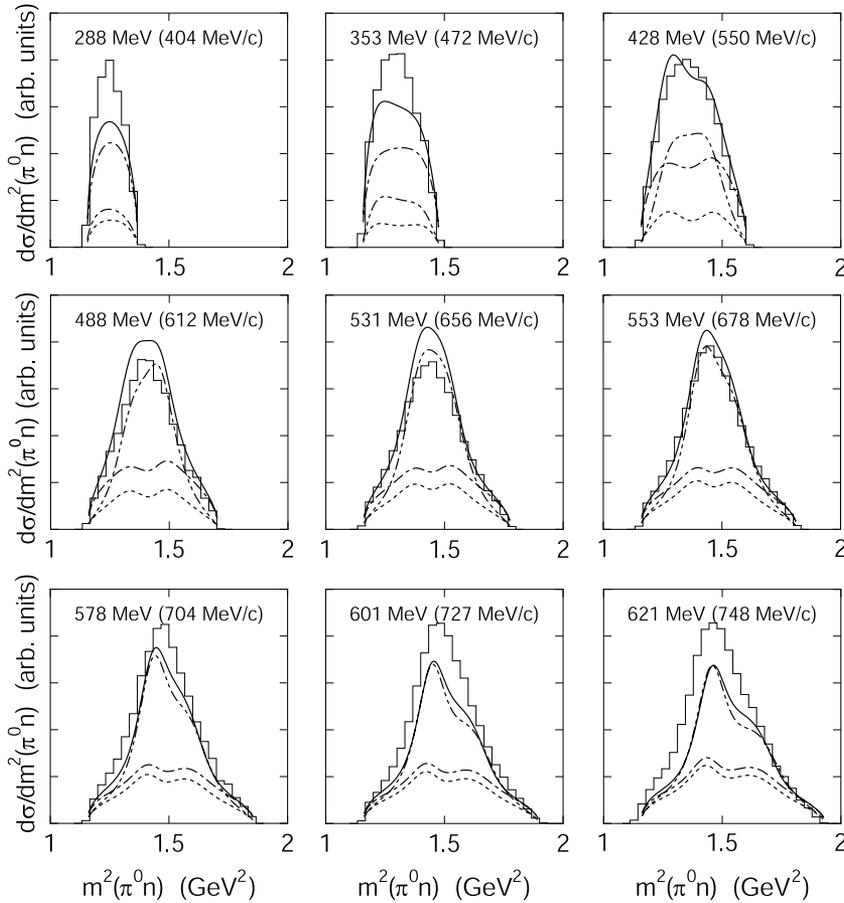
FIG. 11. The $\pi^0 n$ invariant mass distributions for the $\pi^- p \to \pi^0 \pi^0 n$ reaction for several values of T_π (p_π). The CBC data [23] are plotted as the histogram. Each line expresses the results, including (i) all diagrams (solid line), (ii) no $\pi \Delta N^*$ vertex (dotted-dashed line), (iii) no $NN^*(\pi\pi)^{I=0}_{S\,\text{wave}}$ vertex (two-dotted-dashed line), and (iv) neither contribution (dotted line). The $m^2(\pi^0 n) = (1.210)^2 = 1.464$ GeV^2 and $m^2(\pi^0 n) = (1.232)^2 = 1.518$ GeV^2 corresponds to the real part of the $\Delta(1232)$ pole and the Breit-Wigner mass of $\Delta(1232)$, respectively.

Considering all above results, we choose $c_1^* = -8.0$ GeV^{-1} (this leads to $c_2^* = 1.08$ GeV^{-1}) as a plausible value for this parameter.

B. Each contribution of the diagram including $N^*(1440)$

Now we discuss the contribution of each diagram including $N^*(1440)$. The results are shown in Fig. 10. We find that the process Fig. 5(b) gives a negligible contribution for all channels. The process Fig. 5(c) does not give visible influence on the $\pi^+ p \to \pi^+ \pi^+ n$ and $\pi^+ p \to \pi^+ \pi^0 p$ channels but brings 30–50% increase to the total cross section above $T_\pi = 400$ MeV for other three channels.

In the $\pi^- p \to \pi^0 \pi^0 n$ channel, the process including $NN^*(\pi\pi)^{I=0}_{S\,\text{wave}}$ vertex dominates the total cross sections near the threshold, whereas its contribution decreases gradually above $T_\pi = 400$ MeV. Instead the contribution of the process Fig. 5(c) grows in this energy region. We find that the shoulder of the $\pi^- p \to \pi^0 \pi^0 n$ data at the $N^*(1440)$ energy reported in Ref. [23] can be understood as a result of interference between these two processes rather than the sole contribution of $N^*(1440)$ pole.

With regard to the diagrams including $N^*(1440)$, the $\pi^- p \to \pi^+ \pi^- n$ and $\pi^- p \to \pi^0 \pi^0 n$ channels show similar behavior. It is thus expected that the shoulder at $N^*(1440)$ energy may be observed also in the $\pi^- p \to \pi^+ \pi^- n$ channel. To see this, however, more accurate data in those energy region are necessary.

Here we notice that our result underestimates the data above $T_\pi \sim 500$ MeV in the $\pi^- p \to \pi^- \pi^0 p$, $\pi^- p \to \pi^+ \pi^- n$, and $\pi^- p \to \pi^0 \pi^0 n$ channels (particularly remarkable for $\pi^- p \to \pi^- \pi^0 p$). This is not surprising because that energy region is above the Roper mass-shell energy. The higher resonances such as $N^*(1520)$ and $N^*(1535)$, which do not consider in this work, will become relevant to these channels. In particular, $N^*(1520)$ would play a key role because this resonance has a large branching ratio about 45% for the $\pi\pi N$ decay [whereas $N^*(1535)$ has only about the 5% branching ratio]. Indeed, the total cross-section data for these three reaction channels show a small bump around the $N^*(1520)$ energy [see, e.g., Fig. 5(b) and 5(c) in Ref. [1] for the $\pi^- p \to \pi^- \pi^0 p$ and $\pi^- p \to \pi^+ \pi^- n$ channels and the CBC data [23] for $\pi^- p \to \pi^0 \pi^0 n$ channel]. However, such structure is not seen in the $\pi^+ p \to \pi^+ \pi^+ n$ and $\pi^+ p \to \pi^+ \pi^0 p$ channels [see, e.g., Fig. 5(d) and 5(e) in Ref. [1]].

C. Invariant mass distribution of $\pi^- p \to \pi^0 \pi^0 n$ reaction

Figure 11 shows the $\pi^0 n$ invariant mass distributions for several values of T_π. Our result captures the qualitative features of the data well. At $T_\pi = 288$ MeV, the mass distribution is almost determined by the process including $NN^*(\pi\pi)^{I=0}_{S\,\text{wave}}$ vertex. The contribution of this process decreases gradually when T_π becomes higher. Instead, the contribution of the process including $\pi \Delta N^*$ vertex dominates the mass distributions. As suggested in Ref. [23], a peak near the $\Delta(1232)$ energy,
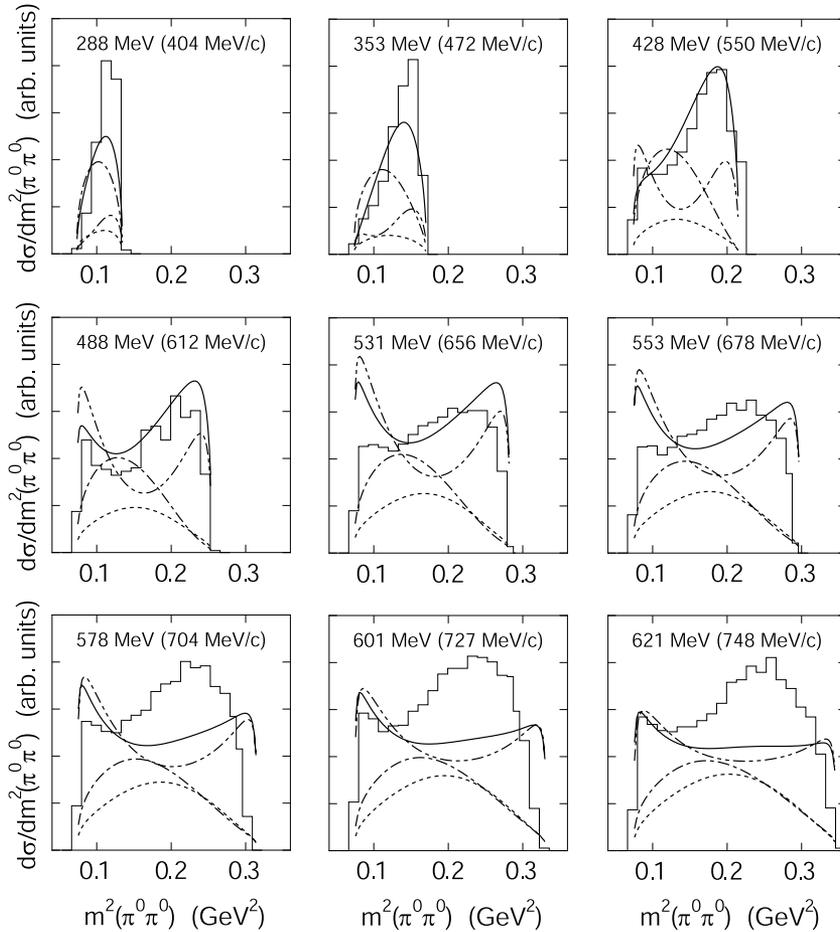
FIG. 12. The $\pi^0\pi^0$ invariant mass distributions for the $\pi^- p \to \pi^0\pi^0 n$ reaction for several values of T_π (p_π). The meaning of each line and histogram is the same as in Fig. 11.

which can be found above $T_\pi = 488$ MeV, is indeed generated by the $N^*(1440) \to \Delta\pi$ process. Although the $\Delta(1232)$ mass is taken as $m_\Delta = 1232$ MeV, the peak occurs at the energy $m^2(\pi^0 n) \simeq (1.210)^2$ GeV^2. In Ref. [23] the authors said that the shift of the peak is natural because the nucleon pole term, which is large background for the πN elastic channel, has small contribution to this reaction. However, in view of our numerical result, we find that the peak position is obtained as a result of the interference of several processes.

We next consider the $\pi^0\pi^0$ invariant mass distribution (Fig. 12). For low T_π, the results are dominated by the process including $NN^*(\pi\pi)^{I=0}_{S\,\mathrm{wave}}$ vertex, which is the same as the case of $\pi^0 n$ invariant mass distribution. We observe that our result reproduces the large asymmetry in the mass distributions around the $N^*(1440)$ energy: a small (large) peak in small (large) value of $m^2(\pi^0\pi^0)$ and a depletion in between (see the result of $T_\pi = 488$ MeV in Fig. 12). In our results, the process with $NN^*(\pi\pi)^{I=0}_{S\,\mathrm{wave}}$ vertex decreases the distribution for small value of $m^2(\pi^0\pi^0)$, whereas it increases for large value of $m^2(\pi^0\pi^0)$. Without this process, the large peak at large value of $m^2(\pi^0\pi^0)$ cannot be reproduced. This result indicates that the large asymmetry in the $\pi^0\pi^0$ mass distribution at the $N^*(1440)$ energy is because of the strong interference between the decay processes $N^*(1440) \to \Delta\pi$ and $N^*(1440) \to N(\pi\pi)^{I=0}_{S\,\mathrm{wave}}$. Our numerical results up to $T_\pi = 500$ MeV agree with the data qualitatively. Above $T_\pi = 500$ MeV, however, our results

do not reproduce a large peak at larger $m^2(\pi^0\pi^0)$. This would be because the contributions of higher mass resonances such as $N^*(1520)$ and $N^*(1535)$ are not taken into account.

It is worth mentioning that the above features of the $\pi^0\pi^0$ and $\pi^0 n$ mass distributions at the $N^*(1440)$ energy are characteristic of the two-pion decay of the Roper resonance, $N^*(1440) \to N\pi\pi$ [13,70]. This indicates that $N^*(1440)$ indeed gives visible effect to the observables of $\pi N \to \pi\pi N$ reaction in those energy region.

D. $I = J = 0$ $\pi\pi$ rescattering in $NN^*(\pi\pi)^{I=0}_{S\,\mathrm{wave}}$ vertex

Finally we discuss the $\pi\pi$ rescattering representing the scalar-isoscalar $\pi\pi$ correlation explicitly in the $NN^*(\pi\pi)^{I=0}_{S\,\mathrm{wave}}$ vertex, which is depicted in Fig. 4(b). It has been suggested in several articles (see, e.g., Refs. [71,72]) that the σ meson pole can be dynamically generated around $450 - 225i$ MeV by such rescattering in $I = J = 0$ channel. In view of the $\pi N \to \pi\pi N$ reaction being sensitive to the process including $NN^*(\pi\pi)^{I=0}_{S\,\mathrm{wave}}$ vertex, we can expect that this reaction also becomes a source of information about this meson. However, no direct evidence of σ meson is seen in the measured data of $\pi^- p \to \pi^0\pi^0 n$ reaction in Ref. [23].

First we try to calculate the $\pi^- p \to \pi^0\pi^0 n$ total cross section *without* the process including $\pi\pi$ rescattering in the $NN^*(\pi\pi)^{I=0}_{S\,\mathrm{wave}}$ vertex, i.e., we consider only the contact
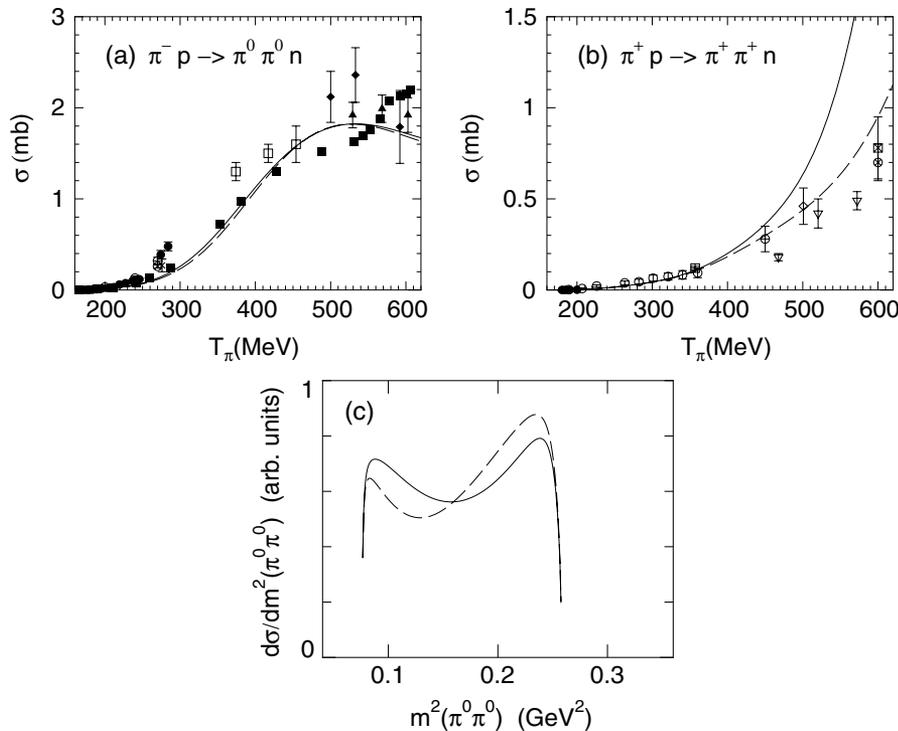
FIG. 13. The $\pi\pi$ rescattering effect in the $\pi N \to \pi\pi N$ reaction: the (a) $\pi^- p \to \pi^0\pi^0 n$ and (b) $\pi^+ p \to \pi^+\pi^+ n$ total cross sections and (c) the $\pi^0\pi^0$ invariant mass distribution of $\pi^- p \to \pi^0\pi^0 n$ at $T_\pi = 488$ MeV. The dashed line is the full result including the $\pi\pi$ rescattering with $(c_1^*, c_2^*) = (-8.0, 1.08)$ GeV^{-1}, whereas the solid line is the result including no $\pi\pi$ rescattering but with the readjusted value $(c_1^*, c_2^*) = (-13.0, 1.89)$ GeV^{-1}.

interaction Fig. 4(a) for this vertex. We find that, even if the $\pi\pi$ rescattering is not considered, we can readjust c_1^* and c_2^* within their allowed values so as to reproduce our results including the $\pi\pi$ rescattering effect.[2] For instance, the total cross section with $c_1^* = -8.0$ [i.e., the solid line in Fig. 9(e)] is reproduced by choosing $c_1^* = -13.0$ and $c_2^* = 1.89$ [see Fig. 13(a)]. The similar results are also obtained for the $\pi^- p \to \pi^+\pi^- n$ and $\pi^\pm p \to \pi^\pm\pi^0 p$ total cross sections and for the $\pi^0 n$ invariant mass distributions of $\pi^- p \to \pi^0\pi^0 n$. Therefore, although the $NN^*(\pi\pi)_{S\,\text{wave}}^{I=0}$ vertex is necessary to explain the $\pi N \to \pi\pi N$ reaction, it seems difficult to conclude whether the σ meson pole dominates the form factors of the vertices as long as we consider only these total cross sections and invariant mass distributions.

However, the situation is somewhat different in the $\pi^+ p \to \pi^+\pi^+ n$ total cross section and the $\pi^0\pi^0$ invariant mass distributions of $\pi^- p \to \pi^0\pi^0 n$. The above value $(c_1^*, c_2^*) = (-13.0, 1.89)$ GeV^{-1} is not acceptable for the $\pi^+ p \to \pi^+\pi^+ n$ total cross section because these values lead to the numerical results far from the data [Fig. 13(b)]. Also, it is remarkable that the large asymmetric shape in the $\pi^0\pi^0$ invariant mass distribution at $T_\pi = 488$ MeV cannot be reproduced without considering the $\pi\pi$ rescattering effect. These results suggest that the $\pi\pi$ rescattering effect in the $NN^*(\pi\pi)_{S\,\text{wave}}^{I=0}$ vertex is *necessary* to our calculation of $\pi N \to \pi\pi N$ reaction.

---

[2]Note that in this case the coefficients in the decay width formula (23) become as $\alpha = 0.476 \times 10^{-3}$ GeV^3, $\beta = 5.29 \times 10^{-3}$ GeV^3, and $\gamma = 2.98 \times 10^{-3}$ GeV^3. Thus the range of allowed values of c_1^* and c_2^* changes.

IV. SUMMARY AND CONCLUSIONS

We have studied the $\pi N \to \pi\pi N$ reaction in the energy region up to $T_\pi = 620$ MeV, especially around the $N^*(1440)$ mass-shell energy. Being motivated by several interesting observations related to $N^*(1440)$ in the recent CBC experiment of the $\pi^- p \to \pi^0\pi^0 n$ reaction, we have discussed the role of $N^*(1440)$ and its decay processes in the reaction processes. The calculation has been performed by extending the theoretical approach constructed in Ref. [13].

We have found that $N^*(1440)$ shows a significant contribution to the $\pi N \to \pi\pi N$ reaction through the decay processes $N^*(1440) \to N(\pi\pi)_{S\,\text{wave}}^{I=0}$ and $N^*(1440) \to \pi\Delta$. In contrast, the $N^* \to \pi N$ process just gives a negligible contribution. Although the contribution of $N^*(1440) \to N(\pi\pi)_{S\,\text{wave}}^{I=0}$ process already appears in the threshold region in several channels, the $N^*(1440) \to \pi\Delta$ process becomes important above $T_\pi = 400$ MeV. The characteristics of the CBC data for $\pi^- p \to \pi^0\pi^0 n$ are generated by a strong interference effect between them.

We have also found that, above $T_\pi = 400$ MeV, the $\pi^+ p \to \pi^+\pi^+ n$ total cross section is remarkably sensitive to the variation of c_1^* and c_2^* within their allowed values. Because this reaction is almost saturated by the contributions of the nucleon and $\Delta(1232)$, more accurate data of this channel would give strong constraints on the range of c_1^* and c_2^*. This nature of $\pi^+ p \to \pi^+\pi^+ n$ cannot be seen in other theoretical studies that have mainly focused on the $\pi N \to \pi\pi N$ reaction below $T_\pi = 400$ MeV.

The remarkable contribution of the process including the $N^* N(\pi\pi)_{S\,\text{wave}}^{I=0}$ vertex leads to the expectation that the $\pi N \to \pi\pi N$ reaction becomes a source of information about

the controversial scalar-isoscalar σ meson. In the present work, the σ meson is considered as a dynamical object generated by the rescattering mechanism of two-pion in the $I = J = 0$ channel. We have obtained the following interesting results related to this meson: if we do not include the $\pi\pi$ rescattering effect in the $N^*N(\pi\pi)^{I=0}_{\text{wave}}$ vertex, then (i) the large asymmetry in the $\pi^0\pi^0$ invariant mass distribution for $\pi^-p \to \pi^0\pi^0 n$ cannot be reproduced and (ii) it is difficult to simultaneously describe the total cross section of all channels. The systematic analyses of all channels would provide an indication of the existence of σ meson.

Here we mention the similarity about the role of $N^*(1440)$ between the $\pi N \to \pi\pi N$ reaction and the NN induced two-pion production reactions. The interference between $N^*(1440) \to N(\pi\pi)^{I=0}_{S\text{ wave}}$ and $N^*(1440) \to \Delta\pi$ is observed also in the $pp \to pp\pi^+\pi^-$ and $pn \to d(\pi\pi)^{I=0}$ reactions [17,18] and actually plays a important role for explaining the data [19,20]. In view of this similarity, we could also discuss the indications of σ meson through those reactions.

Finally, we comment on other baryon resonances related to the $\pi N \to \pi\pi N$ reaction, which have been referred in several places. In the present work, we did not include the higher resonances such as $N^*(1520)$ and $N^*(1535)$. We have seen that, below the $N^*(1440)$ mass-shell energy (i.e., $T_\pi \lesssim 480$ MeV), the $\pi N \to \pi\pi N$ data is almost saturated by the nucleon, $\Delta(1232)$ and $N^*(1440)$. Therefore the higher resonances would become the relevant degrees of freedom at least above $T_\pi \sim 480$ MeV. Several discrepancies between the data and our results above $T_\pi = 500$ MeV in the $\pi^-p \to \pi^-\pi^0 p$, $\pi^-p \to \pi^+\pi^- n$, and $\pi^-p \to \pi^0\pi^0 n$ channels would be cured by the consideration of such higher resonances. Anyway, we need further investigations on these resonances.

APPENDIX A: DETAILS OF THE MODEL IN NUCLEON-Δ SECTOR

As mentioned in Sec. II A, in this appendix we explain some details of the model used in our previous study of $\pi N \to \pi\pi N$ [13]. To calculate the diagrams in Fig. 2, we need to evaluate seven matrix elements shown in Table I.

TABLE I. The matrix elements necessary to calculate the diagrams in Fig. 2.

$\langle N\|j_V\|N\rangle$	$\langle N\|j_A\|N\rangle$	$\langle N\|\hat\sigma\|N\rangle$	$\langle N\|\hat\pi\|N\rangle$
$\langle \Delta\|j_V\|N\rangle$	$\langle \Delta\|j_A\|N\rangle$		
	$\langle \Delta\|j_A\|\Delta\rangle$		

1. Vector-isovector part

The vector current matrix elements are

$\langle N(p')|j^a_{V\mu}(0)|N(p)\rangle$

$$= \bar{u}(p')\left[F^N_{V,1}(t)\gamma_\mu + F^N_{V,2}(t)\frac{i}{2m_N}\sigma_{\mu\nu}q^\nu\right]\frac{\tau^a}{2}u(p) \quad \text{(A1)}$$

for the nucleon, and

$\langle \Delta(p')|j^a_{V\mu}(0)|N(p)\rangle$

$$= \bar{U}^\nu(p')\big[F^{N\Delta}_{V,1}(t)g_{\nu\mu} + F^{N\Delta}_{V,2}(t)Q_\nu\gamma_\mu + F^{N\Delta}_{V,3}(t)Q_\nu Q_\mu$$

$$+ i F^{N\Delta}_{V,4}(t)Q_\nu\sigma_{\mu\lambda}Q^\lambda\big]\gamma_5 I^a(\tfrac{3}{2},\tfrac{1}{2})u(p) \quad \text{(A2)}$$

for the N-Δ transition. In this appendix the isodoublet Dirac spinor for the nucleon is denoted as $u(p)$.

Based on the phenomenology of vector meson dominance (VMD) that at low energy the matrix elements of vector current j_V are dominated by the ρ meson pole, we write the nucleon form factors as

$$F^N_{V,1}(t) = \frac{m^2_\rho}{m^2_\rho - t - im_\rho\Gamma_\rho(t)}, \quad \text{(A3)}$$

$$F^N_{V,2}(t) = \kappa_V F^N_{V,1}(t), \quad \text{(A4)}$$

where m_ρ is the ρ meson mass and κ_V is the isovector magnetic moment. The phenomenological width of the ρ meson is parameterized as

$$\Gamma_\rho(t) = \Gamma_\rho\frac{m_\rho}{\sqrt{t}}\left(\frac{t - 4m^2_\pi}{m^2_\rho - 4m^2_\pi}\right)^{3/2}\theta\big(t - 4m^2_\pi\big), \quad \text{(A5)}$$

where Γ_ρ is the total width at $t = m^2_\rho$ [73]. As for the N-Δ transition form factors, we obtain

$$F^{N\Delta}_{V,1}(t) = \frac{f_{\rho N\Delta}}{f_\rho}\left(\frac{m_N + m_\Delta}{m_\rho}\right)\frac{m^2_\rho}{m^2_\rho - t - im_\rho\Gamma_\rho(t)}, \quad \text{(A6)}$$

$$F^{N\Delta}_{V,2}(t) = \frac{1}{m_N + m_\Delta}F^{N\Delta}_{V,1}(t), \quad \text{(A7)}$$

where we use the $\rho N\Delta$ interaction (B4). The $\rho N\Delta$ coupling constant is denoted as $f_{\rho N\Delta}$, and f_ρ corresponds to the gauge coupling constant of the hidden local symmetry model for the vector mesons [74,75]. The other form factors $F^{N\Delta}_{V,3}(t)$ and $F^{N\Delta}_{V,4}(t)$ in Eq. (A2) are fixed to zero as long as we consider the Lagrangian (B4) for the $\rho N\Delta$ interaction.

2. Axial-isovector part

The matrix elements of j_A are written as [76,77]

$\langle N(p')|j^a_{A\mu}(0)|N(p)\rangle$

$$= \bar{u}(p')\left[F^N_{A,1}(t)\gamma_\mu + F^N_{A,2}(t)q_\mu\right]\gamma_5\frac{\tau^a}{2}u(p), \quad \text{(A8)}$$

$\langle \Delta(p')|j^a_{A\mu}(0)|N(p)\rangle$

$$= \bar{U}^\nu(p')\big[F^{N\Delta}_{A,1}(t)g_{\nu\mu} + F^{N\Delta}_{A,2}(t)Q_\nu\gamma_\mu + F^{N\Delta}_{A,3}(t)Q_\nu Q_\mu$$

$$+ i F^{N\Delta}_{A,4}(t)Q_\nu\sigma_{\mu\lambda}Q^\lambda\big]I^a(\tfrac{3}{2},\tfrac{1}{2})u(p), \quad \text{(A9)}$$

$$\langle \Delta(p') | j^a_{A\mu}(0) | \Delta(p) \rangle$$

$$= \bar{U}^\nu(p') \big[F^\Delta_{A,1}(t) g_{\nu\lambda}\gamma_\mu + F^\Delta_{A,2}(t) g_{\nu\lambda}q^\mu + F^\Delta_{A,3}(t)(q_\nu g_{\mu\lambda}$$

$$+ g_{\nu\mu}q_\lambda) + F^\Delta_{A,4}(t) q_\nu\gamma_\mu q_\lambda + F^\Delta_{A,5}(t) q_\nu q_\mu q_\lambda \big]$$

$$\times \gamma_5 I^a\left(\tfrac{3}{2},\tfrac{3}{2}\right) U^\lambda(p). \tag{A10}$$

Same as in the case of N-N^* and Δ-N^* transitions caused by the axial current j_A, some of the form factors in Eqs. (A8)–(A10) are exactly related to the renormalized coupling constants for the corresponding pion-baryon interaction,

$$f_{\pi NN}(t) = \frac{m_\pi}{f_\pi}\left[\frac{1}{2}F^N_{A,1}(t) + \frac{t}{4m_N}F^N_{A,2}(t)\right], \tag{A11}$$

$$f_{\pi N\Delta}(t) = \frac{m_\pi}{f_\pi}\left[F^{N\Delta}_{A,1}(t) + (m_N - m_\Delta)F^{N\Delta}_{A,2}(t) + tF^{N\Delta}_{A,3}(t)\right], \tag{A12}$$

$$f_{\pi\Delta\Delta}(t) = \frac{m_\pi}{f_\pi}\left[F^\Delta_{A,1}(t) + \frac{t}{2m_\Delta}F^\Delta_{A,2}(t)\right], \tag{A13}$$

where we employ Eqs. (B1)–(B3) as the effective πNN, $\pi N\Delta$, and $\pi\Delta\Delta$ interactions. The other form factors [i.e., $F^{N\Delta}_{A,4}(t)$, $F^\Delta_{A,3}(t)$, $F^\Delta_{A,4}(t)$, and $F^\Delta_{A,5}(t)$] are fixed to zero. In our calculation all the form factors are taken as constants, and we eliminate $F^{N\Delta}_{A,3}$ and $F^\Delta_{A,2}$ by using the PCAC hypothesis $f_{\pi N\Delta,\pi\Delta\Delta}(m^2_\pi) \simeq f_{\pi N\Delta,\pi\Delta\Delta}(0)$.

3. Scalar-isoscalar part

Because $\Delta(1232)$ dose not contribute to $\mathcal{M}_{\text{SA}}$, we only need the nucleon matrix element for the $\hat{\sigma}$ current,

$$\langle N(p') | \hat{\sigma}(0) | N(p) \rangle = S(t)\bar{u}(p')u(p). \tag{A14}$$

According to the definition in Ref. [14], the form factor $S(t)$ is equal to $-\sigma_{\pi N}(t)/f_\pi m^2_\pi$, where $\sigma_{\pi N}(t)$ is the pion-nucleon σ term that becomes independent of t at tree level.

4. Pseudoscalar-isovector part

The nucleon matrix element of the $\hat{\pi}$ current appearing in $\mathcal{M}_\pi$ is written as

$$\langle N(p') | \hat{\pi}^a(0) | N(p) \rangle = P(t)\bar{u}(p')i\gamma_5\tau^a u(p). \tag{A15}$$

The form factor $P(t)$ are related to the renormalized πNN coupling constant (A10),

$$P(t) = \frac{1}{m^2_\pi - t}\left(\frac{2m_N}{m_\pi}\right)f_{\pi NN}(t), \tag{A16}$$

where the pion pole contribution is taken into account.

In Table II, we summarize the constants necessary to calculate the diagrams in Fig. 2.

APPENDIX B: PHENOMENOLOGY OF MESON-BARYON SYSTEM

In this appendix, we summarize the phenomenological Lagrangians used to estimate the form factors and mention a treatment of the finite width of baryon resonances. The

TABLE II. The value of constants used in the previous work. The mass and width of each particle or resonance are shown in MeV.

Masses and widths		Parameters	
m_N	939	f_π	93 MeV
m_π	138	f_ρ	5.80[a]
m_Δ	1232	κ_V	3.71
m_ρ	770	$\sigma_{\pi N}$	45 MeV[b]
Γ_Δ	120	$F^N_{A,1}(= g_A)$	1.265
Γ_ρ	149	$F^N_{A,2}$	5.67×10^{-3} MeV^{-1}[c]
		$F^{N\Delta}_{A,1}$	1.382[d]
		$F^{N\Delta}_{A,2}$	-4.24×10^{-4} MeV^{-1}[d]

[a]See p. 33 in Ref. [75].
[b]Reference [78].
[c]Reference [26]. Note that the relation $F^N_{A,2} = -2\bar{\Delta}_{\pi N}/m^2_\pi$.
[d]Reference [77].

Lagrangians of meson-baryon interaction are written as follows:

$$\mathcal{L}_{\pi NN} = \frac{f_{\pi NN}}{m_\pi}\bar{N}\gamma_\mu\gamma_5\tau^a N \partial^\mu\pi^a, \tag{B1}$$

$$\mathcal{L}_{\pi N\Delta} = \frac{f_{\pi N\Delta}}{m_\pi}\bar{\Delta}^\nu\Theta_{\nu\mu}(Z_1)I^a\left(\tfrac{3}{2},\tfrac{1}{2}\right)N\partial^\mu\pi^a + \text{H.c.}, \tag{B2}$$

$$\mathcal{L}_{\pi\Delta\Delta} = \frac{f_{\pi\Delta\Delta}}{m_\pi}\bar{\Delta}^\alpha\Theta_{\alpha\beta}(Z_2)\gamma_\mu\gamma_5 I^a\left(\tfrac{3}{2},\tfrac{3}{2}\right)$$

$$\times \Theta^\beta{}_\delta(Z_2)\Delta^\delta\partial^\mu\pi^a, \tag{B3}$$

$$\mathcal{L}_{\rho N\Delta} = i\frac{f_{\rho N\Delta}}{m_\rho}\bar{\Delta}^\sigma\Theta_{\sigma\mu}(Z_3)\gamma_\nu\gamma_5 I^a\left(\tfrac{3}{2},\tfrac{1}{2}\right)$$

$$\times N(\partial^\nu\rho^{\mu a} - \partial^\mu\rho^{\nu a}) + \text{H.c.}, \tag{B4}$$

$$\mathcal{L}_{\pi NN^*} = \frac{f_{\pi NN^*}}{m_\pi}\bar{N}\gamma_\mu\gamma_5\tau^a N^*\partial^\mu\pi^a + \text{H.c.}, \tag{B5}$$

$$\mathcal{L}_{\pi\Delta N^*} = \frac{f_{\pi\Delta N^*}}{m_\pi}\bar{\Delta}^\nu\Theta_{\nu\mu}(Z_4)I^a\left(\tfrac{3}{2},\tfrac{1}{2}\right)N^*\partial^\mu\pi^a + \text{H.c.}, \tag{B6}$$

where N and N^*, are the isodoublet Dirac fields describing the nucleon and $N^*(1440)$, respectively, and Δ^μ is the isoquadruplet Rarita-Schwinger field describing the $\Delta(1232)$. The second-rank Lorentz tensor $\Theta_{\mu\nu}$ is defined by $\Theta_{\mu\nu}(Z) \equiv g_{\mu\nu} - \frac{1}{2}(1 + 2Z)\gamma_\mu\gamma_\nu$ (where we take $A = -1$ [79]). The second term of this tensor vanishes if $\Delta(1232)$ is on the mass-shell [because of $\gamma_\mu U^\mu(p) = 0$], and so Z is called the off-shell parameter. In this article we assume $Z_i = -1/2$ ($i = 1\ldots4$) for simplicity, i.e., $\Theta_{\mu\nu} \to g_{\mu\nu}$.

The $\Delta(1232)$ propagator is

$$S_{\mu\nu}(p) = \frac{(\not{p} + m_\Delta)}{3(p^2 - m^2_\Delta)}\left(-2g_{\mu\nu} + \frac{2p_\mu p_\nu}{m^2_\Delta}\right.$$

$$\left. - i\sigma_{\mu\nu} + \frac{\gamma_\mu p_\nu - \gamma_\nu p_\mu}{m_\Delta}\right). \tag{B7}$$

However, the nucleon and $N^*(1440)$ propagators are expressed by the Dirac propagator which is familiar.

To take account of the width of baryon resonances phenomenologically, we modify the denominator of the $\Delta(1232)$ and $N^*(1440)$ propagators as $p^2 - m_R^2 \rightarrow p^2 - m_R^2 + im_R\Gamma_R(s)$, where $R = \Delta$ or N^*. The widths $\Gamma_\Delta(s)$ and $\Gamma_{N^*}(s)$ are taken as [4,5]

$$\Gamma_\Delta(s) = \Gamma_\Delta \frac{m_\Delta}{\sqrt{s}} \frac{|\mathbf{q}(\sqrt{s})|^3}{|\mathbf{q}(m_\Delta)|^3} \theta(\sqrt{s} - m_N - m_\pi), \quad \text{(B8)}$$

and

$$\Gamma_{N^*}(s) = \Gamma_{N^*} \frac{|\mathbf{q}(\sqrt{s})|^3}{|\mathbf{q}(m_{N^*})|^3} \theta(\sqrt{s} - m_N - m_\pi), \quad \text{(B9)}$$

respectively. Here $\mathbf{q} = \mathbf{q}(\sqrt{s})$ is the pion spatial momentum in the center-of-mass πN system with the total energy $\sqrt{s}$. In this article we use $m_{N^*} = 1440$ MeV and $\Gamma_{N^*} = 350$ MeV (as for the value of m_Δ and Γ_Δ, see Table II).

Finally we list the formulas for the isospin matrices used in our calculation (see, e.g., Appendix A in Ref. [5]),

$$I^{a\dagger}\left(\tfrac{3}{2}, \tfrac{1}{2}\right) I^b\left(\tfrac{3}{2}, \tfrac{1}{2}\right) = \delta^{ab} - \tfrac{1}{3}\tau^a\tau^b, \quad \text{(B10)}$$

$$I^{a\dagger}\left(\tfrac{3}{2}, \tfrac{1}{2}\right) I^b\left(\tfrac{3}{2}, \tfrac{3}{2}\right) I^c\left(\tfrac{3}{2}, \tfrac{1}{2}\right)$$
$$= \tfrac{5}{6}i\varepsilon^{abc} - \tfrac{1}{6}\delta^{ab}\tau^c + \tfrac{2}{3}\delta^{ac}\tau^b - \tfrac{1}{6}\delta^{bc}\tau^a. \quad \text{(B11)}$$

[1] D. M. Manley, R. A. Arndt, Y. Goradia, and V. L. Teplitz, Phys. Rev. D **30**, 904 (1984).

[2] D. M. Manley and E. M. Saleski, Phys. Rev. D **45**, 4002 (1992).

[3] R. A. Arndt, W. J. Briscoe, I. I. Strakovsky, R. L. Workman, and M. M. Pavan, Phys. Rev. C **69**, 035213 (2004).

[4] T. S. Jensen and A. F. Miranda, Phys. Rev. C **55**, 1039 (1997).

[5] E. Oset and M. J. Vicente-Vacas, Nucl. Phys. **A446**, 584 (1985).

[6] O. Jäkel, M. Dillig, and C. A. Z. Vasconcellos, Nucl. Phys. **A541**, 675 (1992).

[7] O. Jäkel, H.-W. Ortner, M. Dillig, and C. A. Z. Vasconcellos, Nucl. Phys. **A511**, 733 (1990).

[8] O. Jäkel and M. Dillig, Nucl. Phys. **A561**, 557 (1993).

[9] V. Bernard, N. Kaiser, and U.-G. Meißner, Nucl. Phys. **B457**, 147 (1995).

[10] V. Bernard, N. Kaiser, and U.-G. Meißner, Nucl. Phys. **A619**, 261 (1997).

[11] N. Fettes, V. Bernard, and U.-G. Meißner, Nucl. Phys. **A669**, 269 (2000).

[12] N. Mobed, J. Zhang, and D. Singh, Phys. Rev. C **72**, 045204 (2005).

[13] H. Kamano and M. Arima, Phys. Rev. C **69**, 025206 (2004).

[14] H. Yamagishi and I. Zahed, Ann. Phys. (NY) **247**, 292 (1996).

[15] S. Eidelman et al., Phys. Lett. **B592**, 1 (2004).

[16] L. Alvarez-Ruso, E. Oset, and E. Hernndez, Nucl. Phys. **A633**, 519 (1998).

[17] L. Alvarez-Ruso, Phys. Lett. **B452**, 207 (1999).

[18] L. Alvarez-Ruso, Nucl. Phys. **A684**, 443c (2001).

[19] W. Brodowski et al., Phys. Rev. Lett. **88**, 192301 (2002).

[20] J. Pätzold et al., Phys. Rev. C **67**, 052202(R) (2003).

[21] J. A. Gómez-Tejedor and E. Oset, Nucl. Phys. **A600**, 413 (1996).

[22] K. Craig et al., Phys. Rev. Lett. **91**, 102301 (2003).

[23] S. Prakhov et al., Phys. Rev. C **69**, 045202 (2004).

[24] O. Krehl, C. Hanhart, C. Krewald, and J. Speth, Phys. Rev. C **62**, 025207 (2000).

[25] M. Dillig and M. Schott, nucl-th/0405063.

[26] J. V. Steele, H. Yamagishi, and I. Zahed, Phys. Rev. D **57**, 1703 (1998).

[27] H. Kamano, M. Morishita, and M. Arima, Phys. Rev. C **71**, 045201 (2005).

[28] B. C. Pearce and B. K. Jennings, Nucl. Phys. **A528**, 655 (1991).

[29] G. E. Brown and W. Weise, Phys. Rep. **22**, 279 (1975).

[30] Y. Oh, K. Nakayama, and T.-S. H. Lee, Phys. Rep. **423**, 49 (2006).

[31] M. E. Sevior et al., Phys. Rev. Lett. **66**, 2569 (1991).

[32] G. Kernel et al., Z. Phys. C **48**, 201 (1990).

[33] J. Kirz, J. Schwartz, and R. D. Tripp, Phys. Rev. **126**, 763 (1962).

[34] R. Barloutaud, L. Cardin, A. Derem, C. Gensollen, A. Levèque, C. Louedec, J. Meyer, and D. Tycho, Nuovo Cimento **26**, 1409 (1962).

[35] J. Debaisieux, F. Grard, J. Heughebaert, R. Servranckx, and R. T. V. de walle, Nucl. Phys. **63**, 273 (1965).

[36] M. G. Bowler and R. J. Cashmore, Nucl. Phys. **B17**, 331 (1970).

[37] C. P. Poirier, C. A. Tilger, J. E. D. Alyea, J. H. J. Martin, and J. H. Scandrett, Phys. Rev. **143**, 1092 (1966).

[38] P. C. A. Newcomb, Phys. Rev. **132**, 1283 (1963).

[39] Yu. A. Batusov, S. A. Bunyatov, G. R. Gulkanyan, V. M. Sidorov, M. Musakhanov, G. Ionice, E. Losnianu, V. Mihul, and D. Tuvdendorzh, Sov. J. Nucl. Phys. **21**, 162 (1975).

[40] D. Počanić et al., Phys. Rev. Lett. **72**, 1156 (1994).

[41] M. Arman, D. J. Blasberg, R. P. Haddock, K. C. Leung, B. M. K. Nefkens, B. L. Schrock, D. I. Sober, and J. M. Sperinde, Phys. Rev. Lett. **29**, 962 (1972).

[42] D. H. Saxon, J. H. Mulvey, and W. Chinowsky, Phys. Rev. D **2**, 1790 (1970).

[43] J. A. Jones, W. W. M. Allison, and D. H. Saxon, Nucl. Phys. **B83**, 93 (1974).

[44] T. D. Blokhintseva, V. G. Grebinnik, V. A. Zhukov, G. Libman, L. L. Nemenov, G. I. Selivanov, and Yüan Jung-Fang, Sov. Phys. JETP **15**, 629 (1962).

[45] J. Dolbeau, M. Neveu, F. A. Triantis, and C. Coutures, Nucl. Phys. **B78**, 233 (1974).

[46] M. D. Beer, B. Deler, J. Dolbeau, M. Neveu, N. T. Diem, G. Smadja, and G. Valladas, Nucl. Phys. **12**, 599 (1969).

[47] C. P. Poirier, C. A. Tilger, J. E. D. Alyea, J. H. J. Martin, J. I. Rhode, and J. H. Scandrett, Phys. Rev. **148**, 1311 (1966).

[48] R. A. Burnstein, G. R. Charlton, T. B. Day, G. Quareni, A. Quareni-Vignudelli, G. B. Yodh, and I. Nadelhaft, Phys. Rev. **137**, B1044 (1965).

[49] C. N. Vittitoe, B. R. Riley, W. J. Fickinger, V. P. Kenny, J. G. Mowat, and W. D. Shephard, Phys. Rev. **135**, B232 (1964).

[50] G. Kernel et al., Phys. Lett. **B225**, 198 (1989).

[51] B. C. Barish, R. J. Kurz, V. Perez-Mendez, and J. Solomon, Bull. Am. Phys. Soc. Ser. II **6**, 523 (1961).

[52] A. D. Brody et al., Phys. Rev. D **4**, 2693 (1971).

[53] E. Hernández and E. Oset, Phys. Rev. C **60**, 025204 (1999).

[54] W. A. Perkins, J. C. Caris, R. W. Kenny, and V. Perez-Mendez, Phys. Rev. **118**, 1364 (1960).

[55] J. Deahl, M. Derrick, J. Fetkovich, T. Fields, and G. B. Yodh, Phys. Rev. **124**, 1987 (1961).

[56] C. W. Bjork *et al*., Phys. Rev. Lett. **44**, 62 (1980).

[57] I. M. Blair, H. Müller, G. Torelli, E. Zavattini, and G. Mandrioli, Phys. Lett. **B32**, 528 (1970).

[58] G. Kernel *et al*., Phys. Lett. **B216**, 244 (1989).

[59] Yu. A. Batusov, S. A. Bunyatov, V. M. Sidorov, and V. A. Yarba, Sov. J. Nucl. Phys. **1**, 374 (1965).

[60] T. D. Blokhintseva, V. G. Grebinnik, V. A. Zhukov, G. Libman, L. L. Nemenov, G. I. Selivanov, and Yüan Jung-Fang, Sov. Phys. JETP **17**, 340 (1963).

[61] B. C. Barish, R. J. Kurz, V. Perez-Mendez, and J. Solomon, Phys. Rev. **135**, B416 (1964).

[62] J. K. Kirz, J. Schwartz, and R. D. Tripp, Phys. Rev. **130**, 2481 (1963).

[63] A. A. Bel'kov, S. A. Bunyatov, B. Zh. Zalikhanov, V. S. Kurbatov, A. Khalbaev, and V. A. Yarba, Sov. J. Nucl. Phys. **31**, 96 (1980).

[64] A. V. Kravtsov, A. V. Kuptsov, L. L. Nemenov, E. A. Starchenko, and D. M. Khazins, Sov. J. Nucl. Phys. **20**, 500 (1975).

[65] S. A. Bunyatov, G. V. Zholobov, B. Zh. Zalikhanov, V. S. Kurbatov, M. M. Musakhanov, A. Khalbaev, and V. A. Yarba, Sov. J. Nucl. Phys. **25**, 177 (1977).

[66] A. A. Bel'kov, S. A. Bunyatov, B. Zh. Zalikhanov, V. S. Kurbatov, and A. Khalbaev, Sov. J. Nucl. Phys. **28**, 657 (1978).

[67] J. Lowe *et al*., Phys. Rev. C **44**, 956 (1991).

[68] F. Bulos *et al*., Phys. Rev. **187**, 1827 (1969).

[69] C. B. Chiu *et al*., Phys. Rev. **156**, 1415 (1967).

[70] E. Hernández, E. Oset, and M. J. Vicente Vacas, Phys. Rev. C **66**, 065201 (2002).

[71] N. Kaiser, Eur. Phys. J. A **3**, 307 (1998).

[72] J. A. Oller and E. Oset, Nucl. Phys. **A620**, 438 (1997).

[73] J. V. Steele, H. Yamagishi, and I. Zahed, Nucl. Phys. **A615**, 305 (1997).

[74] M. Bando, T. Kugo, S. Uehara, K. Yamawaki, and T. Yanagida, Phys. Rev. Lett. **54**, 1215 (1985).

[75] M. Harada and K. Yamawaki, Phys. Rep. **381**, 1 (2003).

[76] R. A. Arndt, J. B. Cammarata, Y. N. Goradia, R. H. Hackman, V. L. Teplitz, D. A. Dicus, R. Aaron, and R. S. Longacre, Phys. Rev. D **20**, 651 (1979).

[77] M. Kacir and I. Zahed, Phys. Rev. D **54**, 5536 (1996).

[78] J. Gasser, H. Leutwyler, and M. E. Sainio, Phys. Lett. **B253**, 252 (1991).

[79] L. M. Nath, B. Etemadi, and J. D. Kimel, Phys. Rev. D **3**, 2153 (1971).